# Modeling muscle function using experimentally determined subject-specific muscle properties

**Original Article**

**Title: Modeling muscle function using experimentally determined subject-specific muscle properties.**

**Authors: Wakeling, J.M., Tijs, C., Konow, N., and Biewener, A.A.**

**Author for correspondence:**

James Wakeling, Department of Biomedical Physiology and Kinesiology, Simon Fraser University, Burnaby, BC, Canada
Phone: 778 782 8444
Fax: 778 782 3040
Email: wakeling@sfu.ca

**Word Count: 3483**

Introduction to Discussion, excluding references and equations

**Abstract**

Muscle models are commonly based on intrinsic properties pooled across a number of individuals, often from a different species, and rarely validated against directly measured muscle forces. Here we use a rich data set of rat medial gastrocnemius muscle forces recorded during *in-situ* and *in-vivo* isometric, isotonic, and cyclic contractions to test the accuracy of forces predicted using Hill-type muscle models. We identified force-length and force-velocity parameters for each individual, and used either these subject-specific intrinsic properties, or population-averaged properties within the models. The modeled forces for cyclic *in-vivo* and *in-situ* contractions matched with measured muscle-tendon forces with $r^2$ between 0.70 and 0.86, and root-mean square errors (RMSE) of 0.10 to 0.13 (values normalized to the maximum isometric force). The modeled forces were least accurate at the highest movement and cycle frequencies and did not show an improvement in $r^2$ when subject-specific intrinsic properties were used; however, there was a reduction in the RMSE with fewer predictions having higher errors. We additionally recorded and tested muscle models specific to proximal and distal regions of the muscle and compared them to measures and models from the whole muscle belly: there was no improvement in model performance when using data from specific anatomical regions. These results show that Hill-type muscle models can yield very good performance for cyclic contractions typical of locomotion, with small reductions in errors when subject-specific intrinsic properties are used.

## Introduction

Quantifying muscle forces is necessary for understanding how movements are powered and controlled, yet muscle force is challenging to measure directly during voluntary movements. Some studies have recorded forces from common tendons that originate from multiple muscles (Komi, 1987; Gregor et al. 1987; Hoffer et al. 1987; Biewener and Blickhan, 1988; Finni et al. 2000; Daley and Biewener, 2003); fewer studies have recorded forces directly from distinct tendons (Biewener et al., 1998; Eng et al., 2019; Herzog et al., 1993; Roberts et al., 1997; Walmsley et al., 1978). However, tendon and thus muscle forces for the majority of species, muscles and movements have not yet been recorded; and this is particularly the case for in humans. When muscle forces cannot be directly measured, they are often estimated using computational models (Zajac, 1989). One such model is the Hill-type muscle model that has seen widespread use in more recent years for both *in-situ* (James et al. 1996; Sandercock and Heckman, 1997; Wakeling and Johnson, 1999; Perreault et al. 2003; Wakeling et al. 2012; Millard et al. 2013) and *in-vivo* studies (Hodson-Tole and Wakeling, 2009; Gerus et al. 2012; Lee et al. 2013; Dick et al. 2017). Hill-type muscle models are now embedded in many musculoskeletal simulations of movement to understand muscle use during human movements in health and disease (for review: Seth et al. 2018).

Forces predicted by Hill-type muscle models are sensitive to the intrinsic muscle properties used in the model. Muscles show individual variation in pennation angle (Wickiewicz et al. 1983), muscle quality (isometric stress: Medler, 2002), passive stiffness (Azizi, 2014), intrinsic contraction speed (Sadoyama et al., 1988; Medler 2002), and excitability; with this variation often being caused by ageing (Lauretani et al. 2003), disuse (Narici and de Boer, 2011; Wisdom et al. 2014) and disease (Smith et al. 2019). Previous studies have shown how subject-

specific optimal lengths for fascicles and tendons can improve the accuracy of predicting forces from muscle models (Li et al. 2009; Gerus et al. 2012). However, it is not known how subject-specific fascicle force-length and force-velocity relations would additionally affect the predicted forces, due to the difficulty in measuring these parameters for model validation. In this study we investigate whether the forces predicted by Hill-type muscle models are improved when the models use these subject-specific intrinsic properties. We test these models on *in-vivo* and *in-situ* data obtained from a rat ankle plantarflexor muscle (medial gastrocnemius, MG), a muscle that allows direct measurements of the muscle force from the MG tendon. We test these predictions for contractions over a range of complexity: from *in-situ* isotonic, steady monotonic and cyclic work-loop contractions to unrestrained *in-vivo* locomotion.

Hill-type muscle models are commonly implemented with a single fascicle length and pennation that is assumed to represent the whole muscle that it is emulating (Zajac, 1989). However, skeletal muscles have heterogeneous architecture, and show regional variations in pennation angle, fascicle length, strain, fibre-type properties, and activation (eg. De Ruiter et al 1995, Ahn et al., 2018; Azizi & Deslauriers 2014; Konow et al., 2010). Previously we have shown that Hill-type muscle models that have multiple contractile elements with different intrinsic properties (but the same architecture) predict more accurate forces at high velocity (Lee et al. 2013) and predict reduced metabolic costs of contraction (Lai et al. 2018). It is possible that model refinements that consider the regional differences in architecture may additionally improve the predicted forces. However, this has not been tested against directly measured force. In this study we measure *in-vivo* excitations and length changes in the proximal and distal regions of the rat MG, and test whether the forces predicted from different regions of the muscle would differ, whether they differ from the forces predicted from measures of the whole muscle

87 belly, and how well these predictions match experimentally measured forces on the tendon
88 during *in-situ* and *in-vivo* contractions.

89 We tested the following hypotheses:

90 1) That model-predictions of muscle forces will be worse at the highest contractile
91 frequencies but not the greatest magnitude of force;
92 2) That modeled muscle forces based on subject-specific muscle properties will result in
93 significantly improved predictions of *in-vivo* force patterns compared with forces
94 modeled using muscle properties averaged across a population; and
95 3) That region-specific fiber strain and EMG will result in significantly improved
96 predictions of *in-vivo* forces compared to measures from the whole muscle belly.
97
98

## Methods

*Animals*

All procedures were carried out under approval by the Harvard University (FAS) Institutional Animal Care and Use Committee (protocol 20-09), according to USDA guidelines. Seven male Sprague Dawley rats (body mass: 369±87 g; Table S1) were trained for three weeks, using verbal encouragement and light gusts with an air-duster to locomote at three different gaits/ inclines on a motorized treadmill.

*In vivo measurements*

Each animal was anesthetized (isoflurane gas to effect; 1-2%, via mask). Two sets of bipolar silver wire electromyography (EMG) electrodes and four 1-mm sonomicrometry transducers were inserted into the medial gastrocnemius (MG), and a custom-fabricated 'leaf-spring' force transducer was attached to the MG tendon using sterile surgery procedures (Fig. S1; see (Eng et al., 2019; Konow et al., 2020; Richards and Biewener, 2007). The pairs of sonomicrometry crystals were placed along proximal and distal fascicle axes (8-10mm apart, spanning ~80-85% fascicle length). Misalignment of crystals never exceeded 5°, yielding errors in fascicle strain due to misalignment <1%. The separation of the proximal and distal-most crystals provided measurement of the length of the muscle belly that excluded the tendon. Analgesics (Flunixin meglumine, 2 mg/kg) were administered twice over the 48 hours following surgery.

After surgery recovery, recordings were obtained as animals moved at the steadiest possible speed (walk ~0.3 m $s^{-1}$; trot ~0.8 m $s^{-1}$; gallop ~1.0 m $s^{-1}$) on the level and 14° upslope.

Electrode and transducer signals were sampled at 5 kHz (MP150 16-bit A/D converter, Biopac Systems, Inc., Goleta, CA, USA).

*In-situ measurements*

After *in-vivo* experiments, animals were re-induced on isoflurane gas. A femur clamp was secured to a stereotaxic frame and the foot was zip-tied to a plastic plate on the frame. The MG and the sciatic nerve were exposed using blunt dissection. A cuff electrode (inter-pole spacing of 5.0 mm) was secured around the sciatic nerve, and all sciatic branches distal to the cuff electrode were severed, except for the one innervating MG (Tijs et al., 2014). The calcaneus was cut with the MG tendon intact and attached to the lever arm of a servomotor (Fig. S1A). The muscle and exposed tissue were immersed in mineral oil pooled in a loosened skin flap and regulated at 35±1°C.

Isometric force-length (FL) and isotonic force-velocity (FV) curves were constructed for maximal (amplitude: 2-3 V) and submaximal (amplitude: ~1V) stimulations to the nerve (1.5mA; frequency, 125Hz; pulse width, 0.2ms; train duration: 300ms) via a Grass S48 stimulator. Isotonic shortening contractions relied on servomotor force-control, with contractions crossing the isometric optimal length ($l_0$) for both proximal and distal fascicles. As $l_0$ is affected by muscle activation (Holt and Azizi, 2016; Rack and Westbury, 1969; Rassier et al., 1999), we first determined $l_0$ for each region independently. Three-minute rest periods between successive muscle contractions were used to minimize muscle fatigue. Experimental data were only used for analysis if tetanic force remained ≥90% of the maximum isometric force $F_0$ during the *in-situ* tests.

143 *In-situ* forces from the MG were measured during cyclic work-loop contractions. The
144 muscle length trajectories were set to match those during *in-vivo* upslope gallop strides of a
145 single rat using 3D fluoroscopy (Konow et al., 2020; peak amplitude of 1.2mm and cycle
146 frequency of 3.5Hz); with stimulus onset 60ms before peak MTU length and EMG duty cycle
147 46%, as per *in-vivo* gallop data (Eng et al. 2019). This baseline work-loop condition was then
148 varied in cycle frequency (2 to 10Hz) and peak-to-peak amplitude (0.6 to 2.4mm), with some
149 conditions being low amplitude and high frequency, and others being high amplitude and low
150 frequency. All conditions were recorded for maximal and submaximal stimulations.
151 MG force and EMG signals were sampled at 4kHz; and muscle belly, proximal fascicle,
152 and distal fascicle lengths were sampled at 520Hz via the sonomicrometer. Animals were
153 euthanized after the experiment (pentobarbital sodium overdose, IP). The MG was excised post-
154 mortem, weighed and bisected in the sagittal plane to measure whole muscle belly length and
155 total length of the proximal and distal fascicles, as well as their resting pennation angle $\beta_0$ (Table
156 S1). These measurements were used to correct for the length of fascicles and muscle not spanned
157 by the sonomicrometry crystals. Lastly, tendon transducer output was calibrated to ergometer
158 force measured for a series of *in-situ* isometric tetanic contractions.
159
160 *Modelling isometric and isotonic muscle force*
161 We took the approach of initially determining phenomological relations to describe the
162 intrinsic force-length and force-velocity characteristics of the muscle. We then used these
163 intrinsic properties, combined with measures of the time-varying excitation, length and velocity
164 of the muscle during *in vivo* and *in situ* contractions to predict what the muscle forces would be
165 during these contractions, and compared these predicted forces to independently measured

forces. We used models to predict forces from the muscle belly (using the length and velocity of the muscle belly, and the mean EMG-intensity from both muscle regions), and from either the proximal or distal region of the muscle (using fascicle length and velocity and EMG-intensity from that region).

The peak active force from the FL tests gave the maximum isometric force $F_0$ and the optimal length $l_0$ for the proximal and distal fascicles and the muscle belly. The proximal fascicle, distal fascicle and muscle belly lengths were normalized $\hat{l}$ to their respective optimal lengths for each rat.

The FL data were fit to an active $\hat{F}_a(\hat{l})$ and a passive $\hat{F}_p(\hat{l})$ model (normalized to $F_0$) using least squares minimization:

$$\hat{F}_a(\hat{l}) = e^{-\left|\frac{\hat{l}^w-1}{s}\right|^r} \quad \text{(equation 1)}$$

where $r$ determines roundness, $w$ determines skewness and $s$ determines width of the force-length relationship (Otten, 1985; Hodson-Tole and Wakeling, 2009), and

$$\hat{F}_p(\hat{l}) = e^{(c_1+c_2\hat{l})} \quad \text{(equation 2)}$$

where $c_1$ and $c_2$ are empirical coefficients.

The FV data from the concentric ($\frac{d\hat{l}}{dt} < 0$) isotonic contractions were fit to a piecewise function $\hat{F}_v\left(\frac{d\hat{l}}{dt}\right)$, normalized to $F_0$, using least squares minimization (Lee et al. 2013):

$$\hat{F}_v\left(\frac{d\hat{l}}{dt}\right) = 0 \quad \text{for} \quad \frac{d\hat{l}}{dt} < -1 \quad \text{(equation 3)}$$

$$\hat{F}_v\left(\frac{d\hat{l}}{dt}\right) = \frac{1+\left(\frac{d\hat{l}}{dt}\right)\frac{1}{v_0}}{1-\left(\frac{d\hat{l}}{dt}\right)\frac{1}{kv_0}} \quad \text{for} \quad -1 \le \frac{d\hat{l}}{dt} < 0$$

$$\hat{F}_v\left(\frac{d\hat{l}}{dt}\right) = 1.5 - \frac{0.5\left[1-\left(\frac{d\hat{l}}{dt}\right)\frac{1}{v_0}\right]}{1+7.56\left(\frac{d\hat{l}}{dt}\right)\frac{1}{kv_0}} \quad \text{for} \quad \frac{d\hat{l}}{dt} \ge 0$$

where $k$ is the curvature of the force-velocity relationship, and $v_0$ is the maximum unloaded contraction velocity. For the eccentric portion of the FV curve ($\frac{d\hat{l}}{dt} \geq 0$) curve parameters were taken from Otten (1987): note these parameters were not specific to the individual rats.

An intensity envelope was fit to the EMG signals using an EMG-specific wavelet analysis (Lee et al. 2011). The muscle excitation was taken as the square-root of this EMG-intensity and normalized to the maximum excitation that occurred across all conditions for each recording channel. The excitation was converted to an activation signal using three coupled differential equations as a transfer function (Lee et al. 2011), with rat-specific time-constants calculated from MG twitches recorded in the rat: these were general time-constants fit to pooled data from both proximal and distal EMG-intensities. Muscle activations $\hat{a}(t)$ as a function of time $t$ were calculated separately for the EMG from the proximal and distal locations of the muscle, and the mean of these activations was used to model the forces for the muscle belly.

Muscle forces $F_m$ for both the *in-situ* work-loop and the *in-vivo* locomotion data were calculated as follows:

$$F_m = F_0 \left[\hat{a}(t)\, \hat{F}_a(\hat{l})\hat{F}_v(\frac{d\hat{l}}{dt}) + \hat{F}_p(\hat{l})\right] \hat{F}_\beta$$

We assumed that the thickness of the muscle belly was constant during the experiment (Lee et al. 2013) and calculated it from the post-mortem fiber length and pennation $\beta_0$. The time-varying pennation angle $\beta_i$ was calculated from the fibre length during contraction and belly thickness. Given that the FL properties were measured using the fiber-lengths, but these fibers were already at a pennation angle relative to the line-of-action of the muscle belly, the effect of the time-varying pennation angle $\beta_i$ during contraction was factored in by $\hat{F}_\beta$, where:

$$\hat{F}_\beta = {\mathrm{Cos}(\beta_i)}\Big/{\mathrm{Cos}(\beta_0)}$$

for the force predictions from the proximal and distal fascicles, and

$$\hat{F}_{\beta} = {\mathrm{Cos}(\beta_0)}\Big/{\mathrm{Cos}(\beta_i)}$$

for the force predictions from the muscle belly length.

We separated the *in-situ* data into work-loop cycles, and *in-vivo* data by stride cycles from continuous locomotion bouts that were ~5 seconds long.

**Statistical analysis:**

The predicted muscle forces were evaluated by their coefficient of determination ($r^2$) and root-mean square error (RMSE, relative to $F_0$) by comparison with experimentally measured tendon forces. Values in the text are reported as mean ± standard deviation. All statistical tests used the General Linear Model function in Systat v.12 and involved an initial full-factorial design, factoring individual, modeling method (population based vs. subject-specific), and muscle region. Model-simplifications were carried out when factors were non-significant.

To test **hypothesis 1** we used a nested factorial design to hold either the "force" or "frequency" parameter constant, while testing across conditions for the alternate parameter. Force was dictated *in-vivo* by the treadmill slope condition (Konow et al., 2020), and *in-situ* by sub- or supra-maximal muscle stimulation. Frequency was dictated *in-vivo* by gait condition, and *in-situ* by varying work-loop frequency. Tests were run separately for the *in-situ* and *in-vivo* conditions, and within each condition, for the population average (All) and subject specific (Rat) methods of modeling.

To test **hypothesis 2** we isolated the effect of the method factor to discriminate the effect of using subject-specific (Rat) as opposed to population averages (All) muscle activation and strain-trajectories when modeling muscle force.

To test **hypothesis 3** we used post-hoc testing with pair-wise comparisons of $r^2$ and RMSE for the muscle's proximal and distal regions, and the whole muscle belly.

## Results

Consistent active isometric FL curves were obtained across animals for proximal and distal MG regions, as well as for the whole muscle (Fig. 1A-C). The active FL curve was narrower for the muscle belly compared with the proximal and distal regions. The passive FL curves, however, were more variable across animals (Fig. 1D-F), in large part due to variable disruption of adjacent fascial compartments needed to isolate the MG to obtain *in-situ* FL and FV measurements. For isotonic FV relationships (Fig. 1G-H), the normalized maximum shortening velocities were significantly different between regions ($F_{2,10}$=14.88; p=0.001) without effect of individual ($F_{5,10}$=3.32; p=0.050). Maximum shortening velocities of the muscle belly (5.06±0.98 $s^{-1}$) were lower than for the proximal (10.82±3.01 $s^{-1}$; p<0.01) and distal (9.82±3.22 $s^{-1}$; p<0.05) region, while the difference between the proximal and the distal region was not significant (p>0.05) These FL and FV relations were determined before, and independently of, the evaluation of the Hill-type model force predictions of the cyclic *in situ* contractions and the *in vivo* behaviours.

In general, the time-varying length and activation resulted in excellent model predictions of MG force for both the *in-vivo* locomotor conditions (Fig. 2A-C) and the *in-situ* work-loops (Fig. 2D). However, these model predictions were not as good as for the steady FL and FV data

(Fig. 3). When averaged across the proximal, distal and muscle belly rat-specific models, the mean $r^2$ for the model predictions was 0.996±0.004, 0.857±0.100 and 0.699±0.207 for the steady, cyclic *in-situ*, and *in-vivo* conditions, respectively, and the mean RMSE for the model predictions was 0.016±0.013, 0.101±0.050 and 0.133±0.063 and for the steady, cyclic *in-situ*, and *in-vivo* conditions, respectively. The prediction-accuracy of forces became worse with each increase in *in-vivo* stride frequency (walk to gallop in Figs. 4 and S3) (GLM: $F_{2,1179} = 107.99$; $p<0.001$) and *in-situ* work-loop frequencies (Figs. S2 and S3) ($F_{5,693} = 35.98$; $p<0.001$), but generally exhibited similar or lower $r^2$, and greater RMSE with increased *in-vivo* force as the locomotor grade changed from level to upslope, and increased *in-situ* stimulation intensity.

The quality of model-predictions of forces, as shown by their $r^2$, did not substantially change between models with subject-specific muscle parameters compared to the population means (Fig. 5A). Indeed, the statistical tests for *in-vivo* showed no significant main effect of the model type (subject-specific or population-averaged parameters) on the $r^2$ values ($F_{1.1175} = 0.01$; $p>0.05$), but there was a statistically significant decrease of the RMSE values ($F_{1.1179} = 12.98$; $p<0.001$) for the predicted forces when using subject-specific data (Fig. S3. For *in-situ* work loops, the subject-specific model yielded significantly higher $r^2$ ($F_{1.689} = 57.62$; $p<0.001$). In general, we found that models using the population-averaged parameters predicted forces with higher RMSE errors more often than models that used subject-specific muscle parameters (Fig. 5B).

The model predictions of *in-vivo* force did not improve when using region-specific fiber strain and EMG as compared to the data for the whole muscle belly (Fig. 3). In our population-average (All) modeling approach, averaging proximal and distal activation and using muscle belly length to model the muscle belly forces, in fact, yielded significantly higher $r^2$ than using

regional data collected from distal or proximal compartments ($F_{1,666}$ = 18.39; $p<0.001$). The post-hoc test remained significant for the individual-level comparison ($p<0.001$) despite significant individual variation across the regions. None of the three corresponding RMSE comparisons were statistically significant ($F_{1,666}$ = 0.007; $p>0.05$).

## Discussion

We show here that generally good, to excellent, fits of muscle force can be achieved by muscle models that incorporate subject-specific muscle properties, as well as when properties are pooled across individuals. Rat-specific MG models yielded fits with $r^2$ that ranged from 0.699–0.857 for *in-vivo* locomotor and *in-situ* work-loop contractions to 0.996 for steady FL and FV contractions (Fig. 3), and the RMSE for these rat-specific muscle models ranged from 0.101–0.132 during dynamic *in-vivo* and *in-situ* contractions, respectively, to as low as 0.016 for steady monotonic contractions (relative to $F_{0;}$ Fig. 3).

An important aspect of our modeling approach is that the models were not optimized across all input parameters of the model to achieve a best fit. Instead, we relied on rat-specific values of measured intrinsic muscle properties (active and passive isometric FL, $l_0$, isotonic FV) and fascicle architecture, which were then driven by measured activations (from indwelling EMG) of the muscle during both steady and dynamic *in-vivo* and *in-situ* contractions. Using this approach, we achieved the best predictive fits from Hill-type muscle models to measured muscle forces that have been reported to date. In comparison, prior animal (cat (Perreault et al., 2003; Sandercock and Heckman, 1997); goat (Lee et al., 2013) and human (Dick et al., 2017)) muscle models have achieved fits against measured muscle forces, with $r^2$ ranging from 0.40–0.63 and RMSE ranging from 0.10–0.23 (average ranges when they were reported relative to $F_0$). It

should be noted that the increases in the mean $r^2$ and decreases in mean RMSE were larger than their median values, due to the skewed nature of the distributions of $r^2$ and RMSE. Not only did the mean and median measures improve with the rat-specific intrinsic properties (Fig. 5), but there was a reduction in the skewness of the distributions, with a reduction in the number of cases of poor model fits when compared to models that used population-averaged intrinsic properties.

A large source of variability, and likely error, arising from our rat MG model was the considerable experimental variation in $l_0$ and passive FL properties measured for the MG across individual rats (Fig. 1D-F, Table 2). The resting length for elastic tissues, including tendons, is often assumed to occur at muscle $l_0$. Passive muscle stiffness strongly influences the time-varying force predicted by a muscle model in relation to activation and changes in muscle length (Thelen, 2003; Li et al. 2009; Gerus et al. 2012, 2015). Nevertheless, despite the considerable variation in resting length that we observed across individual muscle preparations, which likely reflected the unavoidable disruption of fascial compartments to obtain *in-situ* measurements of muscle properties (Tijs et al. 2020), the models predicted good fits (Fig. 2) for dynamic changes in force during *in-situ* work-loop and *in-vivo* locomotion contractions.

The predicted muscle forces showed worse fits ($r^2$) and greater errors (RMSE) for the higher cycle and stride frequencies, in a manner consistent with previous reports for cyclic contractions (James et al. 1996; Wakeling and Johnston 1999, Dick et al. 2017). This speed-sensitivity may reflect the increasing importance of time-sensitive processes such as deactivation rates (Askew and Marsh, 1998) as cycle durations become shorter. Whilst errors appear greater for upslope versus level *in-vivo* gait, and maximal versus submaximal *in-situ* stimulations, it should be noted that these errors are all relative to the maximal isometric force: the errors

relative to the peak force during each contraction cycle were less for cycles that generated greater force. The greater $r^2$ values for level *versus* upslope locomotion may reflect the more complex patterns of muscle fascicle strain during upslope locomotion, where the muscle experiences periods of both active lengthening and active shortening (Fig. 2; Eng et al. 2019; Konow et al., 2020). Active lengthening of a muscle likely incurs history-dependent effects that are not captured by the steady FL and FV properties used in Hill-type models. When a muscle develops force with prior active lengthening its force may be elevated compared to its isometric force at the same length (Abbott and Aubert 1952; Cavagna and Citterio 1974; Edman et al. 1982; Herzog and Leonard 2002; Hisey et al. 2009), and force may be reduced when the muscle reaches that length with prior active shortening (Abbott and Aubert 1952; Marechal and Plaghki 1979; Meijer et al. 1998; Herzog et al. 2000). These history-dependent effects may be included in models of muscle force (Rode et al. 2009; Herzog et al. 2012; Herzog 2014; Nishikawa et al. 2012, McGowan et al. 2013; Ross et al. 2018); however, most current Hill-type models do not consider contraction history and so there is still scope for increasing model accuracy. Whilst accounting for active lengthening is important for eccentric contractions, the amount of active lengthening was small for these typical gaits in the rat and thus the scope for such model improvement is limited in this case.

Our modelled MG forces did not improve when region-specific length and EMG data were used, rather than muscle belly length and mean EMG intensity across the muscle. This possibly reflects the complexity and heterogeneity of the architecture and recruitment within the rat MG. Additionally, the supramaximal stimulation of the sciatic nerve for the *in situ* contractions will have induced the same recruitment for the two regions, reducing the scope for region-specific differences in force. It would seem that the whole muscle output cannot

necessarily be predicted from one isolated region, but rather will emerge from the outputs and interactions between the different muscle regions.

We were surprised to find, therefore, that modelled forces did not statistically improve when subject-specific intrinsic properties were used compared to the models with more generic population-averaged parameters: this may partly reflect the very good model fits that were already achieved with the generic models. However, it should be noted that the muscle models with subject-specific models were more likely to achieve lower errors than the generic model. Consequently, for clinical assessments there may be considerable merit in using patient-specific parameters for muscle models, which may deviate more substantially from the distribution of values across a healthy population.

**Acknowledgements**

We thank Pedro Ramirez for husbandry care of the rats. This work was funded by the National Institutes of Health [5R01-AR055648 to A.A.B. and J.M.W.].

**Declaration of Competing Interest**

The authors declare that they have no known competing financial interests or personal relationships that could have appeared to influence the work reported in this paper.

**References**

Abbott, B. C., Aubert, X. M., 1952. The force exerted by active striated muscle during and after change of length. Journal of Physiology 117, 77–86.

Ahn A.N., Konow N., Tijs C., and Biewener A.A., 2018. Different Segments within Vertebrate Muscles Can Operate on Different Regions of Their Force–Length Relationships. Integrative and Comparative Biology 58: 219-231.

Askew, G. N., Marsh, R. L., 1998. Optimal shortening velocity (V/Vmax) of skeletal muscle during cyclical contractions: length-force effects and velocity-dependent activation and deactivation. Journal of Experimental Biology 201, 1527–1540.

Azizi E., Deslauriers A.R., 2014. Regional heterogeneity in muscle fiber strain: The role of fiber architecture. Frontiers in Physiology 5: 303.

Azizi, E., 2014. Locomotor function shapes the passive mechanical properties and operating lengths of muscle. Proceedings of the Royal Society B: Biological Sciences, 281(1783), 20132914. doi:10.1098/rspb.2013.2914

Biewener, A. A., Blickhan, R., 1988. Kangaroo rat locomotion: design for elastic energy storage or acceleration? Journal of Experimental Biology 140, 243-255.

Biewener, A. A., Konieczynski, D. D., Baudinette, R. V., 1998. In vivo muscle force-length behavior during steady-speed hopping in tammar wallabies. Journal of Experimental Biology, 201, 1681-1694.

Cavagna, G. A., Citterio, G., 1974. Effect of stretching on the elastic characteristics and the contractile component of frog striated muscle. Journal of Experimental Biology 239, 1–43.

Daley, M. A., Biewener, A. A., 2003. Muscle force-length dynamics during level versus incline locomotion: a comparison of in vivo performance of two guinea fowl ankle extensors. Journal of Experimental Biology, 206, 2941-2958.

De Ruiter C.J., De Haan A., Sargeant A.J., 1995. Physiological characteristics of two extreme muscle compartments in gastrocnemius medialis of the anaesthetized rat. Acta Physiologica Scandinavica 153: 313-324.

Dick, T. J. M., Biewener, A. A., Wakeling, J. M., 2017. Comparison of human gastrocnemius forces predicted by Hill-type muscle models and estimated from ultrasound images. Journal of Experimental Biology, 220, 1643-1653.

Edman, K. A., Elzinga, G., Noble, M. I., 1982. Residual force enhancement after stretch of contracting frog single muscle fibers. The Journal of General Physiology, 80, 769–784.

Eng, C. M., Konow, N., Tijs, C., Holt, N. C., Biewener, A. A., 2019. In vivo force–length and activation dynamics of two distal rat hindlimb muscles in relation to gait and grade. Journal of Experimental Biology, 222, jeb205559, doi:10.1242/jeb.205559.

Finni, T., Komi, P.V., Lepola, V., 2000. In vivo human triceps surae and quadriceps femoris muscle function in a squat jump and counter movement jump. European Journal of Applied Physiology, 83(4-5), 416–426. doi:10.1007/s004210000289

Gerus, P., Rao, G., Berton, E., 2012. Subject-Specific Tendon-Aponeurosis Definition in Hill-Type Model Predicts Higher Muscle Forces in Dynamic Tasks. PLoS One, 7(8), e44406. doi:10.1371/journal.pone.0044406

Gerus, P., Rao, G., Berton, E., 2015. Ultrasound-based subject-specific parameters improve fascicle behaviour estimation in Hill-type muscle model. Computer Methods in Biomechanics and Biomedical Engineering, 18, 116–123. doi:10.1080/10255842.2013.780047

411 Gregor, R. J., Komi, P. V., & Järvinen, M, 1987. Achilles tendon forces during cycling.
412 International Journal of Sports Medicine, 8 Suppl 1, 9–14.
413 Herzog, W., 2014. The role of titin in eccentric muscle contraction. Journal of Experimental
414 Biology, 217, 2825–2833. doi:10.1242/jeb.099127
415 Herzog, W., Leonard, T. R., 2002. Force enhancement following stretching of skeletal muscle: a
416 new mechanism. Journal of Experimental Biology, 205, 1275–1283.
417 Herzog, W., Leonard, T. R., Guimaraes, A. C. S., 1993. Forces in gastrocnemius, soleus and
418 plantaris muscles for the freely moving cat. Journal of Biomechanics, 26, 945-953.
419 Herzog, W., Leonard, T. R., Guimaraes, A. C. S., 1993. Forces in gastrocnemius, soleus and
420 plantaris muscles for the freely moving cat. Journal of Biomechanics 26, 945-953.
421 Herzog, W., Leonard, T. R., Wu, J. Z., 2000. The relationship between force depression
422 following shortening and mechanical work in skeletal muscle. Journal of
423 Biomechanics, 33, 659–668.
424 Herzog, W., Leonard, T., Joumaa, V., DuVall, M., Panchangam, A., 2012. The three filament
425 model of skeletal muscle stability and force production. Molecular and Cellular
426 Biomechanics, 9, 175–191.
427 Hisey, B., Leonard, T. R., Herzog, W., 2009. Does residual force enhancement increase with
428 increasing stretch magnitudes? Journal of Biomechanics, 42, 1488–1492.
429 doi:10.1016/j.jbiomech.2009.03.046
430 Hodson-Tole, E. F., Wakeling, J. M., 2009. The influence of strain and activation on the
431 locomotor function of rat ankle extensor muscles. Journal of Experimental Biology,
432 213, 318–330. doi:10.1242/jeb.031872

433 Hoffer, J.A., Loeb, G.E., Sugano, N., Marks, W.B., O'Donovan, M.J., Pratt, C.A.,1987. Cat
434 hindlimb motoneurons during locomotion. III. Functional segregation in sartorius.
435 Journal of Neurophysiology, 57(2), 554–562. doi:10.1152/jn.1987.57.2.554
436 Holt, N. C., Azizi, E., 2016. The effect of activation level on muscle function during locomotion:
437 are optimal lengths and velocities always used? Proceedings of the Royal Society of
438 London B: Biological Sciences, 283, 20152832.
439 James, R. S., Young, I. S., Cox, V. M., Goldspink, D. F., and Altringham, J. D., 1996. Isometric
440 and isotonic muscle properties as determinants of work loop power output. Pflugers
441 Archiv - European Journal of Physiology, 432, 767–774.
442 Komi, P.V., 1990. Relevance of in vivo force measurements to human biomechanics. Journal of
443 Biomechanics, 23, 23–34. doi:10.1016/0021-9290(90)90038-5
444 Konow N., Thexton A., Crompton A.W., German R.Z., 2010. Regional differences in length
445 change and electromyographic heterogeneity in sternohyoid muscle during infant
446 mammalian swallowing. Journal of Applied Physiology 109: 439-448.
447 Konow, N., Collias, A., Biewener, A. A., 2020. Skeletal muscle shape change in relation to
448 varying force requirements across locomotor conditions. Frontiers in Physiology, 11,
449 143.
450 Lai, A. K. M., Biewener, A. A., Wakeling, J. M., 2018. Metabolic cost underlies task-dependent
451 variations in motor unit recruitment. Journal of the Royal Society Interface, 15(148),
452 20180541. doi:10.1098/rsif.2018.0541
453 Lauretani, F., Russo, C., Bandinelli, S., Bartali, B., Cavazzini, C., Di Iorio, A., et al., 2003. Age-
454 associated changes in skeletal muscles and their effect on mobility: an operational
455 diagnosis of sarcopenia. Journal of Applied Physiology, 95, 1851-1860.

456 Lee, S. S. M., Arnold, A. S., Miara, M. de B., Biewener, A. A., Wakeling, J. M., 2013. Accuracy
457 of gastrocnemius muscles forces in walking and running goats predicted by one-
458 element and two-element Hill-type models. Journal of Biomechanics, 46, 2288–2295.
459 doi:10.1016/j.jbiomech.2013.06.001
460 Lee, S. S. M., de Boef Miara, M., Arnold, A. S., Biewener, A. A., Wakeling, J. M., 2011. EMG
461 analysis tuned for determining the timing and level of activation in different motor
462 units. Journal of Electromyography and Kinesiology, 21, 557–565.
463 doi:10.1016/j.jelekin.2011.04.003
464 Li, L., K.Y. Tong, K.Y., X.L., Hu, X.L., Hung, L.K., and Koo, T.K.K., 2009. Incorporating
465 ultrasound-measured musculotendon parameters to subject-specific EMG-driven
466 model to simulate voluntary elbow flexion for persons after stroke. Clinical
467 Biomechanics, 24, 101–109. doi:10.1016/j.clinbiomech.2008.08.008
468 Marechal ,G., Plaghki, L., 1979. The deficit of the isometric tetanic tension redeveloped after a
469 release of frog muscle at a constant velocity. Journal of General Physiology, 73, 453–
470 67.
471 McGowan, C. P., Neptune, R. R., Herzog, W., 2013. A phenomenological muscle model to
472 assess history dependent effects in human movement. Journal of Biomechanics, 46,
473 151–157. doi:10.1016/j.jbiomech.2012.10.034
474 Medler, S., 2002. Comparative trends in shortening velocity and force production in skeletal
475 muscles. American Journal of Physiology-Regulatory, Integrative and Comparative
476 Physiology, 283, R368–R378.

Meijer, K., Grootenboer, H.J., Koopman, H.F., Van Der Linden, B.J., Huijing, P.A., 1998. A Hill type model of rat medial gastrocnemius muscle that accounts for shortening history effects. Journal of Biomechanics, 31, 555–63.

Millard, M., Uchida, T., Seth, A., Delp, S. L., 2013. Flexing Computational Muscle: Modeling and Simulation of Musculotendon Dynamics. Journal of Biomechanical Engineering, 135(2), 021005. Doi:10.1115/1.4023390

Narici, M. V., de Boer, M. D., 2011. Disuse of the musculo-skeletal system in space and on earth. Eurpoean Journalof Applied Physiology, 111, 403–420. doi:10.1007/s00421-010-1556-x

Nishikawa, K., Monroy, J., Uyeno, T., Yeo, S., Pai, D., Lindstedt, S., 2012. Is titin a "winding filament?" A new twist on muscle contraction. Proceedings of the Royal Society B: Biological Sciences, 279, 981-990.

Otten, E., 1985. The jaw mechanism during growth of a generalised Haplochromis species: H. elegans Trewavas 1933 (Pisces, Cichlidae). Netherlands Journal of Zoology, 33, 44-98.

Otten, E., 1987. A myocybernetic model of the jaw system of the rat. Journal of Neuroscience Methods, 21, 287-302.

Perreault, E. J., Heckman, C. J., Sandercock, T. G., 2003. Hill muscle model errors during movement are greatest within the physiologically relevant range of motor unit firing rates. Journal of Biomechanics, 36, 211-218.

Rack, P. M., Westbury, D. R., 1969. The effects of length and stimulus rate on tension in the isometric cat soleus muscle. Journal of Physiology, 204, 443-60.

499 Rassier, D. E., MacIntosh, B. R., Herzog, W., 1999. Length dependence of active force
500 production in skeletal muscle. Journal of Applied Physiology, 86, 1445-1457.
501 Roberts, T. J., Marsh, R. L., Weyand, P. G., Taylor, C. R., 1997. Muscular force in running
502 turkeys: the economy of minimizing work. Science, 275, 1113-1115.
503 Rode, C., Siebert, T., Blickhan, R., 2009. Titin-induced force enhancement and force depression:
504 A "sticky-spring" mechanism in muscle contractions? Journal of Theoretical Biology,
505 259, 350–360. doi:10.1016/j.jtbi.2009.03.015
506 Ross, S. A., Ryan, D. S., Dominguez, S., Nigam, N., Wakeling, J. M., 2018. Size, History-
507 Dependent, Activation and Three-Dimensional Effects on the Work and Power
508 Produced During Cyclic Muscle Contractions. Integrative and Comparative Biology,
509 58, 232-250. doi:10.1093/icb/icy021
510 Sadoyama, T., Masuda, T., Miyata, H., Katsuta, S., 1988. Fibre conduction velocity and fibre
511 composition in human vastus lateralis. European Journal of Applied Physiology, 57,
512 767-771.
513 Sandercock, T. G., Heckman, C. J., 1997. Force from cat soleus muscle during imposed
514 locomotor-like movements: Experimental data versus Hill-type model predictions.
515 Journal of Neurophysiology 77, 1538-1552.
516 Seth, A., Hicks, J. L., Uchida, T. K., Habib, A., Dembia, C. L., Dunne, J. J., et al., 2018.
517 OpenSim: Simulating musculoskeletal dynamics and neuromuscular control to study
518 human and animal movement. PLoS Computational Biology, 14(7), e1006223.
519 doi:10.1371/journal.pcbi.1006223
520 Smith, L. R., Pichika, R., Meza, R. C., Gillies, A. R., Baliki, M. N., Chambers, H. G., Lieber, R.
521 L., 2019. Contribution of extracellular matrix components to the stiffness of skeletal

522 muscle contractures in patients with cerebral palsy. Connective Tissue Research, 1–12.
523 doi:10.1080/03008207.2019.1694011
524 Thelen, D. G., 2003. Adjustment of Muscle Mechanics Model Parameters to Simulate Dynamic
525 Contractions in Older Adults. Journal of Biomechanical Engineering, 125, 70-77.
526 Tijs, C., Konow, N., Biewener, A. A., 2020. Effect of muscle stimulation intensity on the
527 heterogeneous function of compartments within an architecturally complex muscle.
528 Journal of Applied Physiology (revised).
529 Tijs, C., van Dieën, J. H., Baan, G. C., Maas, H., 2014. Three-Dimensional Ankle Moments and
530 Nonlinear Summation of Rat Triceps Surae Muscles. PLoS ONE 9, e111595.
531 Wakeling, J. M., Johnston, I., 1999. Predicting muscle force generation during fast-starts for the
532 common carp Cyprinus carpio. Journal of Comparative Physiology B: Biochemical,
533 Systemic, and Environmental Physiology, 169, 391–401.
534 Wakeling, J. M., Lee, S. S. M., Arnold, A. S., de Boef Miara, M., Biewener, A. A., 2012. A
535 Muscle's Force Depends on the Recruitment Patterns of Its Fibers. Annals of
536 Biomedical Engineering, 40, 1708–1720. doi:10.1007/s10439-012-0531-6
537 Walmsley, B., Hodgson, J. A., Burke, R. E., 1978. Forces produced by medial gastrocnemius and
538 soleus muscles during locomotion in freely moving cats. Journal of Neurophysiology.
539 41, 1203-1216.
540 Wickiewicz, T., Roy, R., Powell, P., Edgerton, V., 1983. Muscle architecture of the human lower
541 limb. Clinical Orthopaedics and Related Research, 179, 275-283.
542 Wisdom, K. M., Delp, S. L., Kuhl, E., 2014. Use it or lose it: multiscale skeletal muscle
543 adaptation to mechanical stimuli. Biomechanics and Modeling in Mechanobiology, 14,
544 195–215. doi:10.1007/s10237-014-0607-3

545 Zajac, F., 1989. Muscle and tendon: properties, models, scaling, and application to biomechanics
546 and motor control. Critical Reviews in Biomedical Engineering, 17, 359–410.
547

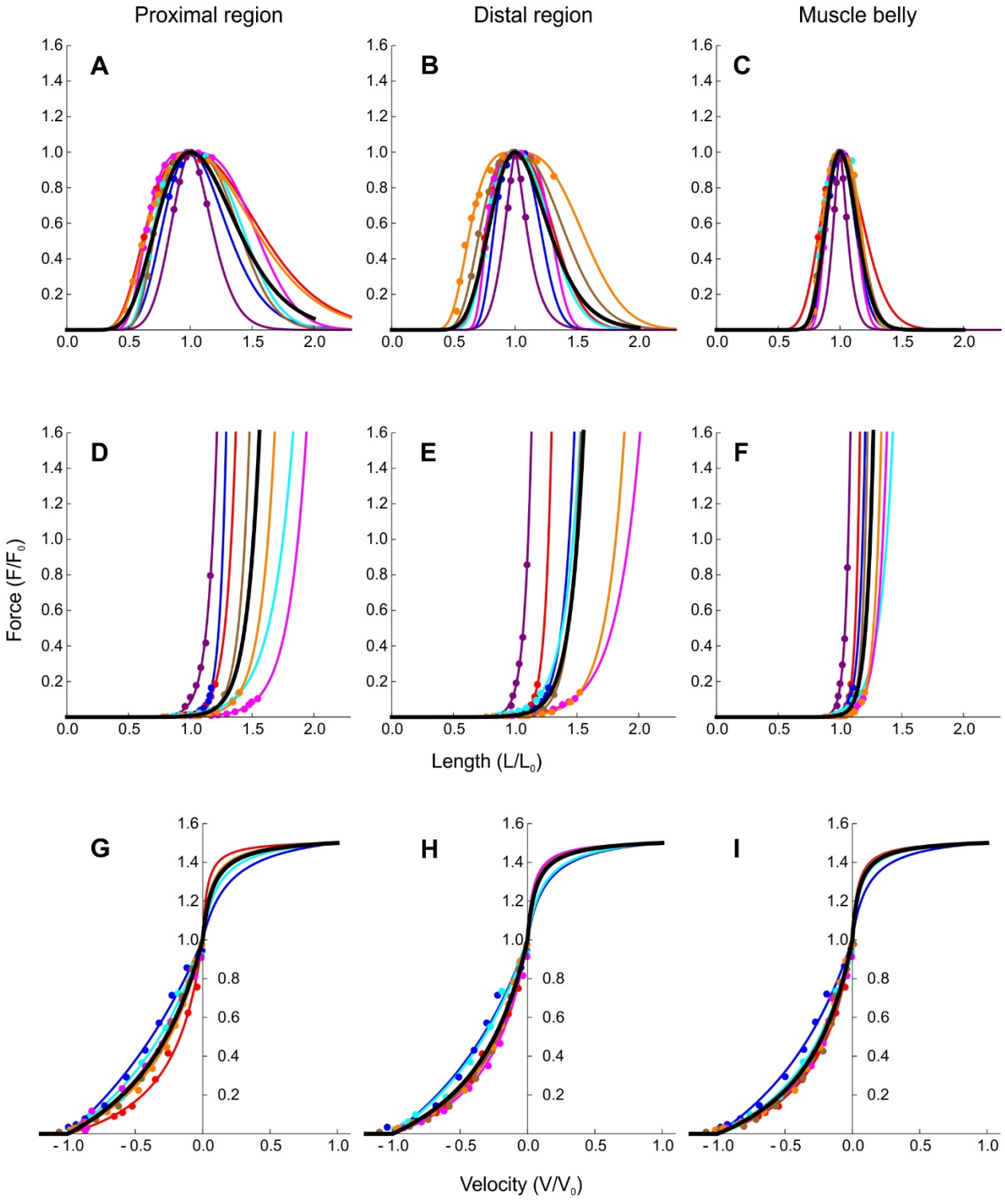


**Fig. 1. Isometric force-length (active A-C; passive (D-F), and isotonic force-velocity (G-I) relations for the rat medial gastrocnemius.** Individual rats are distinguished by color (experimental data: points and fitted models: lines). The pooled FL and FL curves (black lines) were fit to all the data across the different individuals.

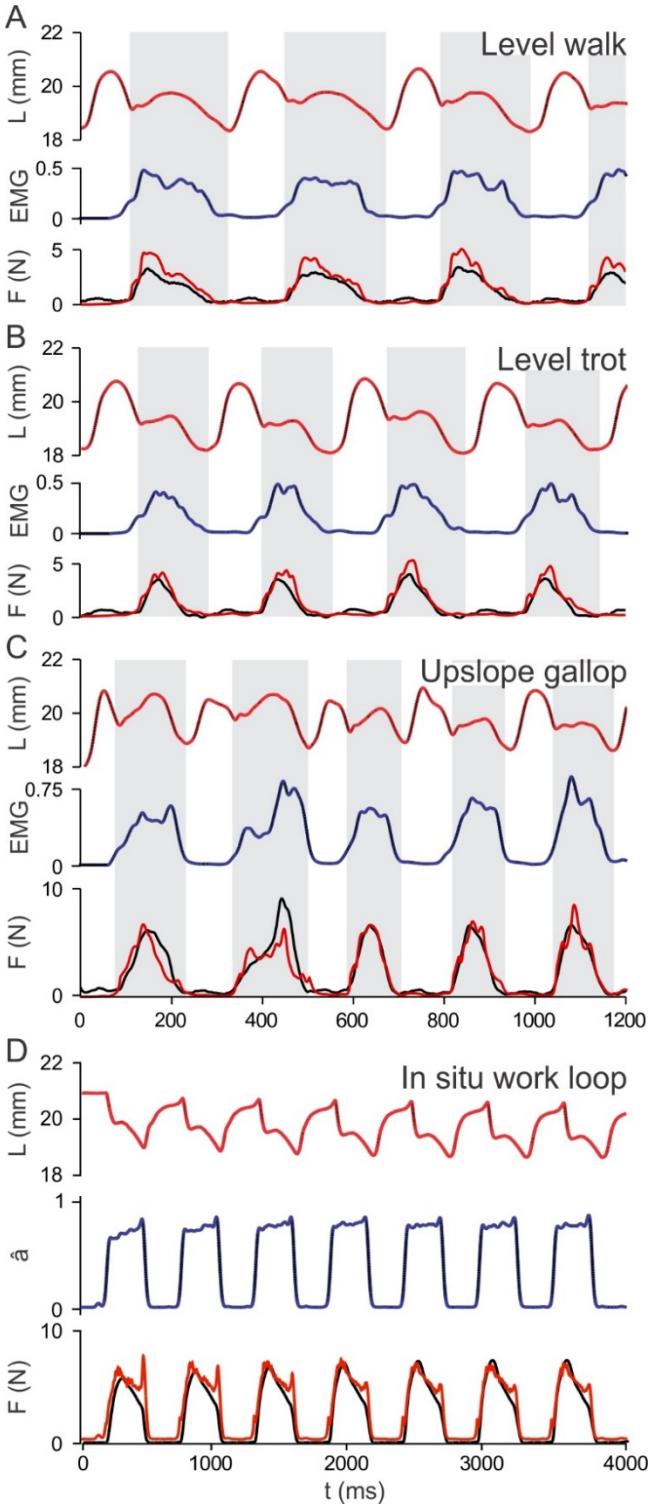


**Fig. 2. Rat MG length, EMG and forces for *in-vivo* locomotion (A-C) and *in-situ* work-loop recordings.** Length is from the sonomicrometry measures of the muscle belly. EMG-intensity (*in-vivo*) or activation (*in-situ*) is pooled between the proximal and distal sites. Forces were measured at the tendon (black) or predicted from the muscle models (red lines).

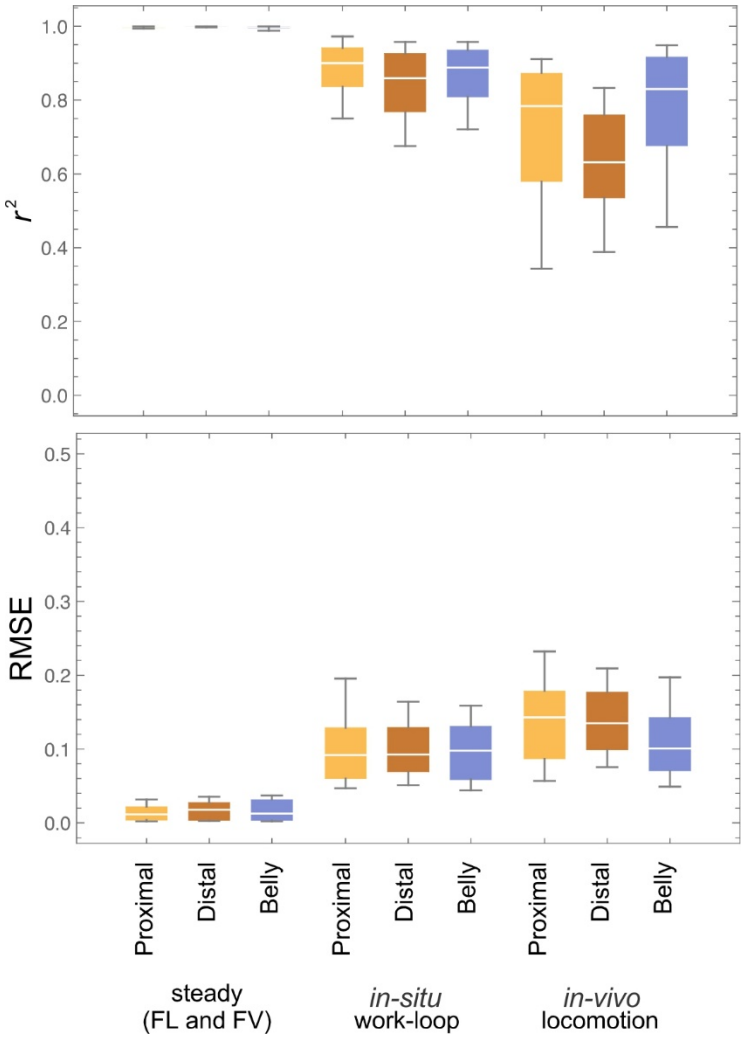


**Fig. 3. Summary box plots ($r^2$ and RMSE) comparing quality of modelled forces when using rat-specific intrinsic properties in the models.** Box plots show median values with 25/75 quartiles, and whiskers delineating the 90% quartile ranges.

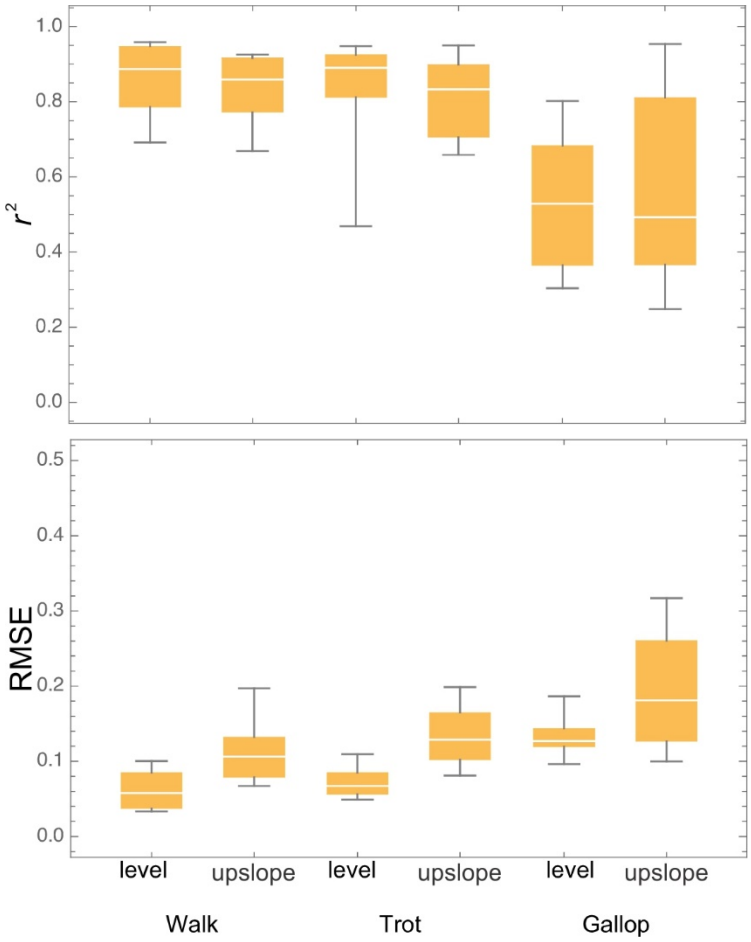


**Fig. 4. Box plots ($r^2$ and RMSE) across *in-vivo* conditions averaged for the whole muscle belly.** Data are taken for the whole muscle belly. These models using rat-specific intrinsic properties yielded forces with lower $r^2$ and higher RMSE for gallop compared with trotting and walking conditions (see Fig. S3 for statistical evaluation). RMSE was generally higher for upslope gait versus level gait conditions. Box plots show median values with 25/75 quartiles, and whiskers delineating the 90% quartile ranges.

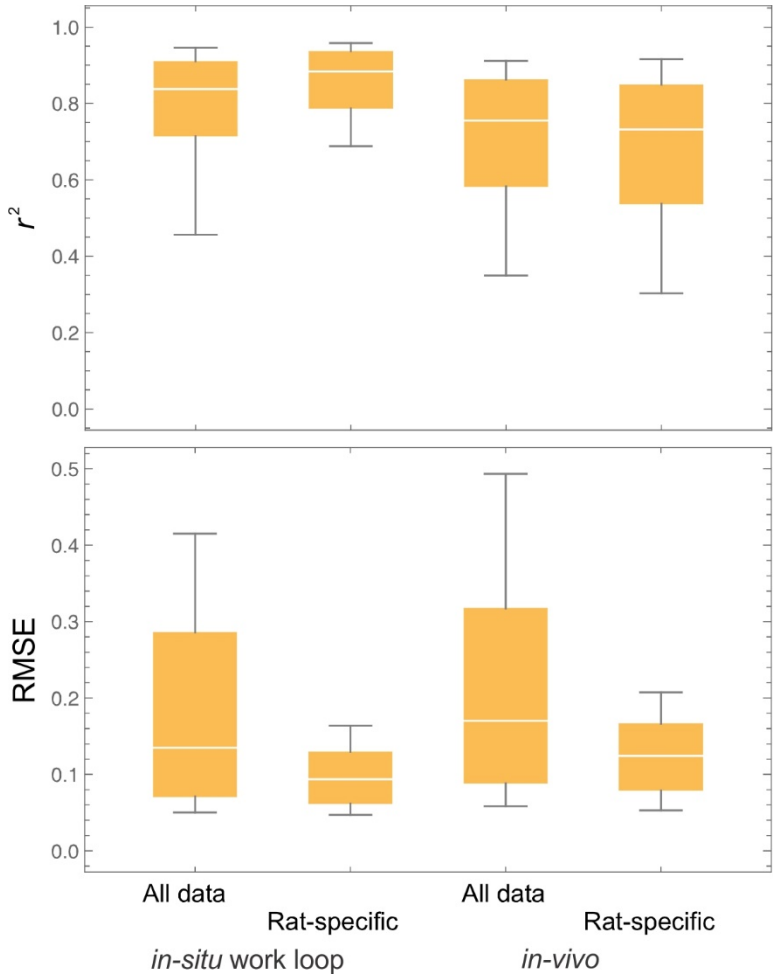


**Fig. 5. Summary box plots ($r^2$ and RMSE) across steady versus dynamic *in-situ* work-loop and *in-vivo* conditions.** Note how the models using intrinsic properties pooled across the population of rats had model fits with higher RMSE than compared to models with rat-specific properties. Box plots show median values with 25/75 quartiles, and whiskers delineating the 90% quartile ranges.

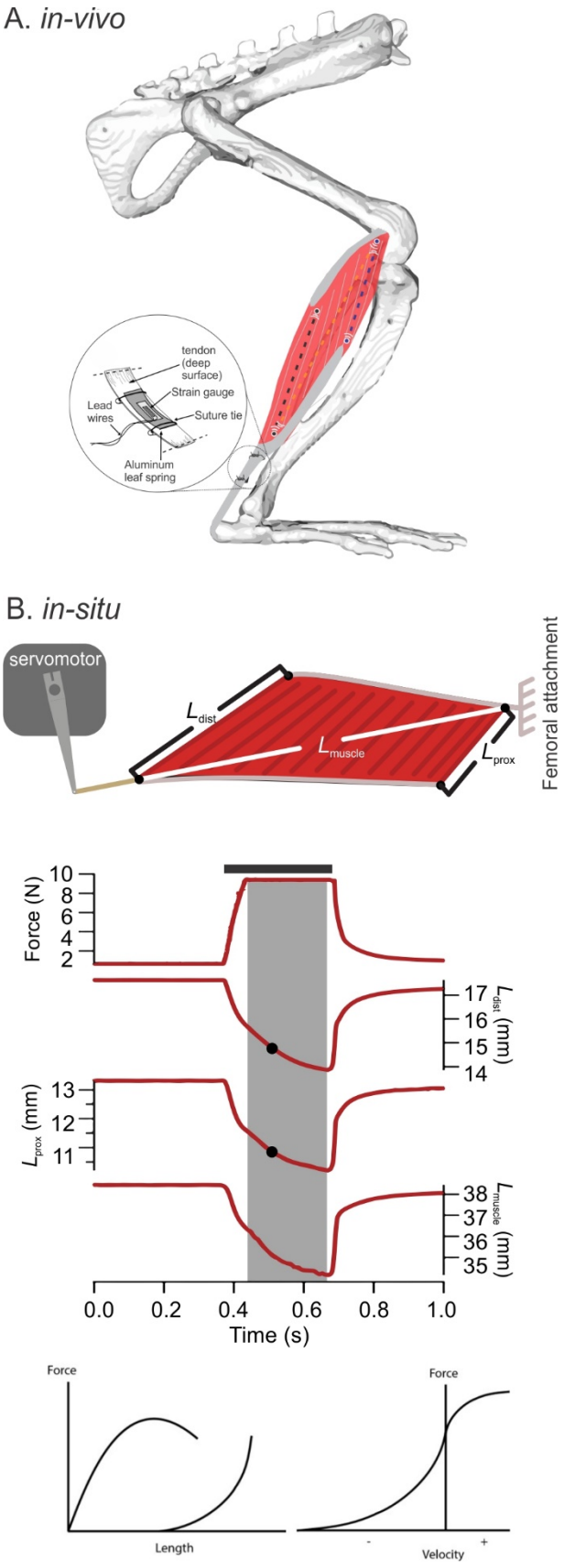
A. in-vivo
tendon (deep surface)
Strain gauge
Lead wires
Suture tie
Aluminum leaf spring
B. in-situ
servomotor
$L_{dist}$
$L_{muscle}$
$L_{prox}$
Femoral attachment
Force (N)
10
8
6
4
2
17
16
15
14
$L_{dist}$ (mm)
13
12
11
$L_{prox}$ (mm)
38
37
36
35
$L_{muscle}$ (mm)
0.0
0.2
0.4
0.6
0.8
1.0
Time (s)
Force
Length
Force
-
+
Velocity

576

**Fig. S1. Schematic of (A) *in-vivo* and (B) *in-situ* force and length measurements.** (A) *In-vivo* MG forces were recorded using a leaf-spring force transducer surgically attached to the free MG tendon (Richards and Biewener, 2007; Eng et al. 2019). Proximal and distal fascicle length changes, as well as whole muscle belly length were recorded using 1.0 mm sonomicrometry crystals, along with fine-wire EMG electrodes implanted in both regions (not shown). (B) *In-situ* MG forces were measured by isolating the MG tendon and calcar attachment to a lever-based ergometer, with the proximal origin of the muscle remaining attached to the femur, which was fixed by a clamp. Stimulation of the muscle via the sciatic nerve elicited tetanic FL and FV contractions under supramaximal (2-3 v) and submaximal (~1 v) conditions, allowing active and passive FL and isotonic FV curves to be constructed.

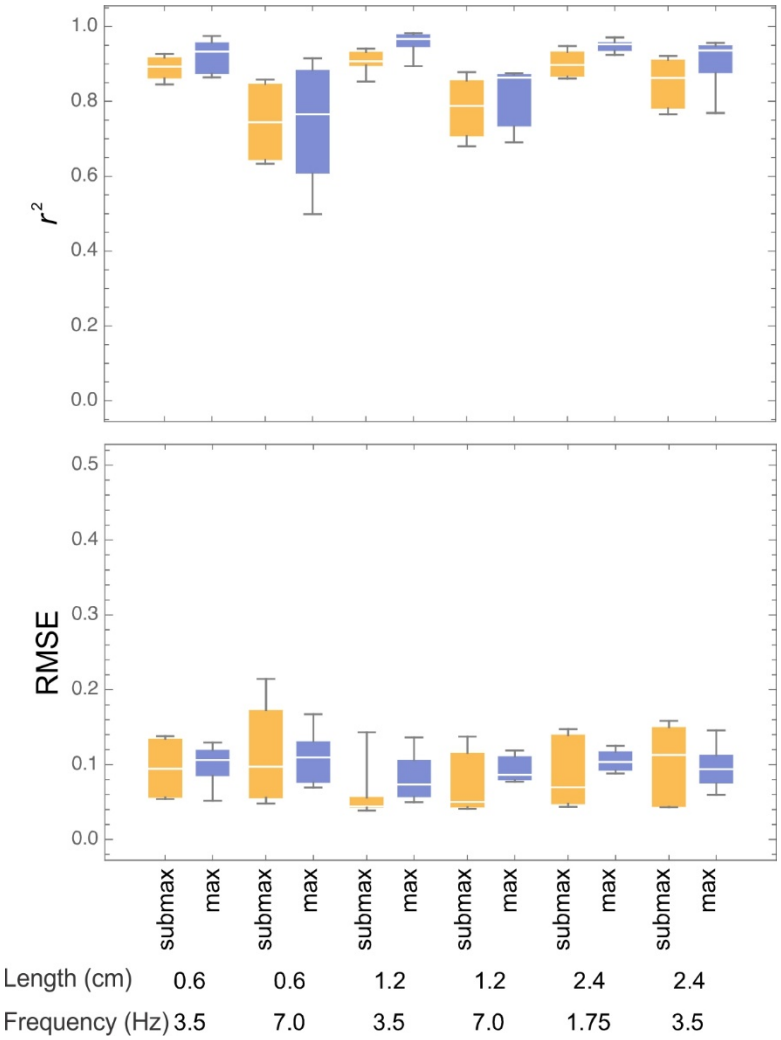


**Fig. S2. Box plots ($r^2$ and RMSE) comparing quality of modelled forces when using rat-specific intrinsic properties in the models across *in-situ* work-loop conditions (Δlength & frequency) for the whole muscle belly.** Predictive fits of rat-specific muscle models to forces measured during *in-situ* work-loops were generally similar across the range of imposed lengths and frequencies, with $r^2$ averaging 0.88±0.10 and RMSE averaging 0.09±0.04. No significant difference in RMSE or $r^2$ was observed for model fits to supramaximal versus submaximal intensity work-loops (Fig. S3). Box plots show median values with 25/75 quartiles, and whiskers delineating the 90% quartile ranges.

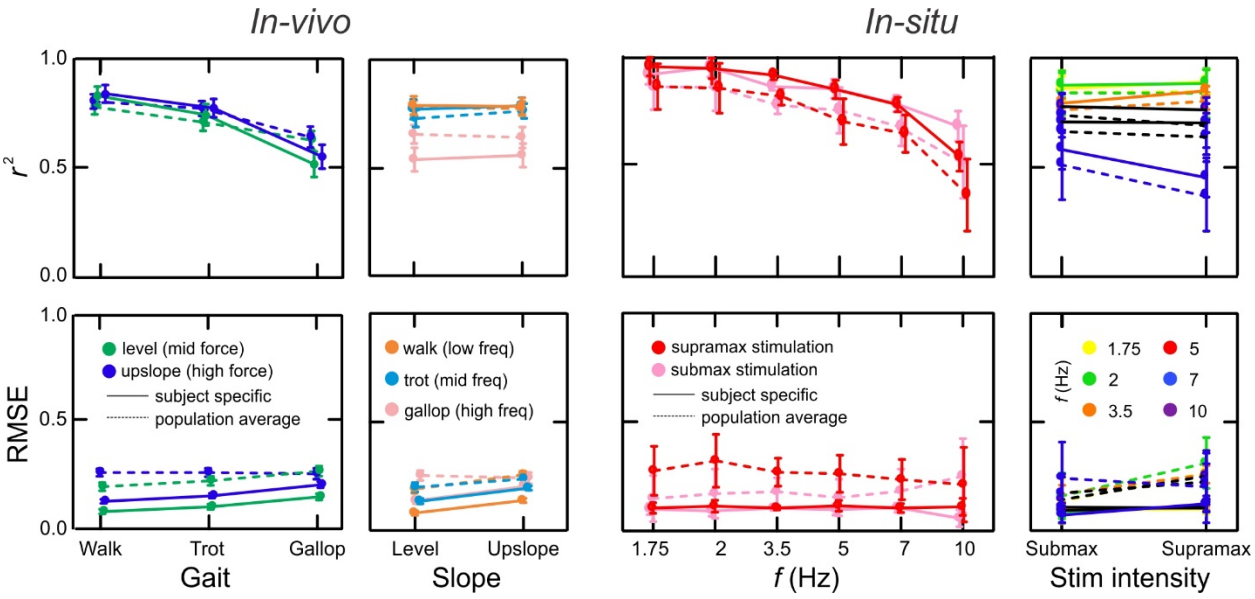


**Fig. S3. Least-Square Means plots** summarizing the statistical results related to testing hypothesis 1; that model-predictions of muscle forces will be less accurate at the highest contractile frequencies but not the greatest magnitude of force. For both *in-vivo* (Left) and *in-situ* (Right), we used a nested factorial design to keep either the "force" or "frequency" parameter constant, while testing across conditions for the alternate parameter. Force was dictated *in-vivo* by the treadmill slope condition (Konow et al., 2020), and *in-situ* by sub- or supra-maximal muscle stimulation. Frequency was dictated *in-vivo* by gait condition, and *in-situ* by varying work-loop frequency. Within each condition, tests were run separately for the population average and subject specific model inputs. Results are largely consistent across conditions, with $r^2$ values being significantly reduced by increasing cycle frequency but remaining largely invariant by changes in force. RMSE values are generally better for modeling based on population average data. For statistical test results, please see the results section.

614

**Table 1. Active FL parameters.** See equation 1. Rat-specific parameters are shown as mean±SD.

| | | $r$ | $w$ | $S$ | $l_0$ [mm] | $F_0$ [N] | $r^2$ | RMSE |
|---|---|---|---|---|---|---|---|---|
| Proximal | Pooled | 2.37 | 0.217 | 0.475 | 8.57 | 8.52 | 0.857 | 0.128 |
| | Rat | 2.83 ±0.75 | 0.206 ±0.256 | 0.501 ±0.691 | 8.74 ±2.45 | 9.88 ±6.26 | 0.998 ±0.002 | 0.013 ±0.007 |
| Distal | Pooled | 2.29 | 0.135 | 0.417 | 9.48 | 8.54 | 0.732 | 0.209 |
| | Rat | 2.93 ±0.78 | 0.091 ±0.159 | 0.289 ±0.592 | 9.14 ±3.03 | 9.89 ±6.27 | 0.994 ±0.012 | 0.019 ±0.012 |
| Belly | Pooled | 2.17 | 0.096 | 0.567 | 22.0 | 8.56 | 0.846 | 0.125 |
| | Rat | 2.57 ±0.50 | 0.079 ±0.204 | 0.477 ±1.236 | 21.9 ±3.1 | 9.90 ±6.26 | 0.994 ±0.006 | 0.019 ±0.012 |

615

616

617

618

**Table 2. Passive FL parameters.** See equation 2. Rat-specific parameters are shown as mean±SD.

| | | $c_1$ | $c_2$ | $r^2$ | RMSE |
|---|---|---|---|---|---|
| Proximal | Pooled | -13.0 | 7.74 | 0.021 | 0.329 |
| | Rat | -14.3±4.2 | 9.26±4.11 | 0.997±0.003 | 0.005±0.006 |
| Distal | Pooled | -12.3 | 7.44 | 0.040 | 0.308 |
| | Rat | -14.1±4.6 | 9.26±4.51 | 0.998±0.001 | 0.006±0.009 |
| Belly | Pooled | -21.3 | 16.7 | 0.079 | 0.185 |
| | Rat | -23.8±7.0 | 19.3±6.72 | 0.995±0.007 | 0.008±0.012 |

619

620

621

622

**Table 3. FV parameters.** See equation 3. Rat-specific parameters are shown as mean±SD.

| | | $k$ | $v_0$ [$s^{-1}$] | $r^2$ | RMSE |
|---|---|---|---|---|---|
| Proximal | Pooled | 0.802 | 10.82 | 0.983 | 0.064 |
| | Rat | 1.24±1.20 | 10.82±3.01 | 0.998±0.002 | 0.027±0.013 |
| Distal | Pooled | 0.638 | 9.82 | 0.989 | 0.051 |
| | Rat | 0.775±0.473 | 9.82±3.22 | 0.997±0.002 | 0.028±0.011 |
| Belly | Pooled | 0.509 | 5.06 | 0.989 | 0.051 |
| | Rat | 0.599±0.391 | 5.06±0.98 | 0.997±0.002 | 0.026±0.014 |

623

624

625

626

627

628

**Table S1. Measurements from the subjects used in this study**.

| Rat | Body mass (g) | MG mass (g) | $l_{muscle}$ (mm) | Proximal $l_{fascicle}$ (mm) | Distal $l_{fascicle}$ (mm) | Proximal $\theta_{fascicle}$ (deg) | Distal $\theta_{fascicle}$ (deg) |
|---|---|---|---|---|---|---|---|
| 1 | 207 | 0.446 | 19.1 | 6.7 | 8 | 27 | 19 |
| 2 | 247 | 0.673 | 27.6 | 6.8 | 8.3 | 20 | 15 |
| 3 | 289 | 0.719 | 29.1 | 7.8 | 8.9 | 21 | 17 |
| 4 | 362 | 0.976 | 33.2 | 8.8 | 10.3 | 22 | 17 |
| 5 | 380 | 1.035 | 31.8 | 8.4 | 10.3 | 25 | 21 |
| 6 | 360 | 0.911 | 30.1 | 7.9 | 9.6 | 21 | 20 |

629

630

631